Arch. Metall. Mater. **66** (2021), 1, 321-330

DOI: 10.24425/amm.2021.134790

ZHU YONGMEI[1], CHEN JUNJIE[1], TANG WENXIAN[1], CUI WEICHENG[2,3],
WANG XIAORONG[1], WANG FANG[2*], YIN BAOJI[1]

FATIGUE AND CORROSION FATIGUE OF 18Ni MARAGING STEEL

This study focused on the fatigue and corrosion fatigue of maraging steel 18Ni (250). The 18Ni (250) samples were tested for axial fatigue in air and 3.5% NaCl solution. The effects of loading frequency and stress ratio on the fatigue strength of 18Ni (250) were studied. In air, the loading frequency was 10 Hz, and the stress ratio was 0.5. However, three loading methods were used in the 3.5% NaCl solution: (i) the loading frequency of 1 Hz and stress ratio of 0.5; (ii) the loading frequency of 1 Hz and stress ratio 0.1, and (iii) the loading frequency 5 Hz and stress ratio 0.5. The corrosion fatigue strength of samples in the 3.5% NaCl solution was 63.3% lower than that of the samples in air. The fractures in the samples were observed after the test.

Keywords: corrosion fatigue, 18Ni (250), loading frequency, stress ratio, 3.5%NaCl solution

1. Introduction

Fatigue is the phenomenon in which materials crack or even fracture due to cyclic stress or strain. In fact, fatigue failure of the structures in the petrochemical industry and offshore structures is mostly in the form of corrosion fatigue, in which cracks initiate and propagate due to cyclic loading in a corrosive environment [1,2]. Offshore structures are vulnerable to corrosion fatigue due to the harsh marine environment and this may lead to significant levels of damage to the structures and hence a reduction in service life [3,4]. To reduce the occurrence of damage, studying the effect of corrosion fatigue on different materials is crucial.

The factors affecting the corrosion fatigue of high strength steel are mainly material factor, environmental factor and mechanical factor. Guslyakova et al. [5] studied the effect of properties of deformed structural steel on fatigue failure resistance. It was found that the corrosion fatigue resistance tended to vary after plastic deformation of the steels in relation to their strain capacity. Chapman et al. [6] studied the effect of temperature on corrosion fatigue. It was found that the corrosion fatigue crack propagation rate increased with the increase of temperature. Of course, loading conditions cannot be ignored, loading frequency and stress ratio have different effect on corrosion fatigue. Researchers found that the effect of frequency on fatigue life was negligible in air at room temperature when frequency was between 1 and 100 Hz [7,8]. However, in a corrosive solution, the frequency was an important factor affecting the corrosion fatigue crack propagation rate [9-12]. Strizak et al. [8] studied the effect of frequency on the 316LN stainless steel fatigue behavior under various test conditions. They founded that fatigue life decreased with frequency decreasing in mercury. Colombo et al. [9] studied the corrosion fatigue behavior of hydrogen pre-charged low alloy Cr-Mo steel and proposed that the corrosion fatigue crack propagation rate decreased by half order of magnitude when the frequency increased by one order of magnitude. The grain size of metal or passivation film on the surface affected the progress of corrosion fatigue, while, loading frequency is synergistic with corrosion, so the effect of frequency on corrosion fatigue behavior is closely related to material properties. May et al. [10] found that a frequency in the range from 10 to 120 Hz had no appreciable effect on the corrosion fatigue crack initiation life of X12CrMoV12-3 martensitic stainless steel in a solution containing 0.1 M NaCl and 0.044 M Na_2SO_4 with pH = 6. This effect was observed because the repassivation rate was significantly lower than the characteristic time of the strain from the applied cyclic stress at a frequency in the range of 10 to 120 Hz. In contrast to frequency, the stress ratio of cyclic loading affects the fatigue behavior in the air and corrosive environ-

[1] JIANGSU UNIVERSITY OF SCIENCE AND TECHNOLOGY, COLLEGE OF MECHANICAL ENGINEERING, ZHENJIANG 212003, CHINA
[2] SHANGHAI OCEAN UNIVERSITY, SHANGHAI ENGINEERING RESEARCH CENTER OF HADAL SCIENCE AND TECHNOLOGY, COLLEGE OF MARINE SCIENCES, SHANGHAI 201306, CHINA
[3] WESTLAKE UNIVERSITY, SCHOOL OF ENGINEERING, HANGZHOU 310024, CHINA
* Corresponding author: wangfang@shou.edu.cn

ments [13,14]. However, the effect was based on the material properties, sample shapes, and loading conditions. Sivaprasad et al. [15] conducted a corrosion fatigue crack propagation test of high-strength steel HSLA in air and the 3.5% NaCl solution. They found that the corrosion fatigue crack propagation rate increased with an increase in R at medium and large ΔK values. However, the effect of R was not significant at small ΔK, where ΔK represents the stress intensity factor.

Maraging steel attracts the attention of designers who design deep ocean submersibles due to its extremely high strength that satisfies the design requirements of manned cabins or water ballast tanks. Especially, according to a preliminary investigation and study, 18Ni maraging steels are widely used due to their application history, performance, and current manufacturing capabilities [16]. Moreover, 18Ni (250) maraging steel has an ultra-high strength, thus making it an alternative material for fabricating a full ocean depth pressure hull [17]. Few studies have carried out on the corrosion fatigue behavior of 18Ni (250) and the effect of frequency and stress ratio on the fatigue strength of 18Ni (250).

In this study, the fatigue and corrosion fatigue behaviors of 18Ni (250) at room temperature were studied, and the effect of loading frequency and stress ratio on the fatigue behavior was investigated. The fatigue life and fatigue strength of 18Ni (250) were assessed based on the test results with the change in the loading frequency and stress ratio in air and 3.5% NaCl solution. The fracture surface was observed and spectrum analysis was taken after conducting the tests.

2. Materials and Methods

The test material was high-strength 18Ni (250) maraging steel. After conducting an aging heat treatment on the sample, the hardness of 18Ni (250) was up to 50-52 HRC, and the deformation caused by heat treatment was minimal. The as-received material was initially in the solid solution state without any heat treatment. The chemical composition is presented in Table 1, which was provided by the manufacturer. Material machining was conducted in the solid solution state before the aging heat treatment. The temperature and time of the aging heat treatment would influence the microstructure and strength of 18Ni (250). In this study, the best aging heat treatment method was selected with the following parameters – temperature: 482°C and time: 3 h.

2.1. Mechanical property test

The sample of mechanical property test was a round rod, and the shape and sizes are presented in Fig. 1. The sample gauge was polished with emery paper, and the polishing direction was parallel to the axial direction of the sample. To ensure an accurate result, the test was conducted thrice on different samples. The three samples obtained were termed as #1, #2, and #3, and the testing section diameters of the samples were 5.99, 6.01, and 6.01 mm, respectively. The tensile tests of mechanical properties were conducted at room temperature in accordance with the Chinese standard GB/T228.1-2010, and the entire test process was completed on an electronic universal testing machine. To determine the deformation in the samples during the testing process, an extensometer was used.

The test results include five parameters – yield strength, Young's modulus, ultimate tensile strength, area reduction, and elongation. Fig. 2 displays the force-strain curve of the three samples. 18Ni (250) had no obvious yield process. Therefore, the stress value corresponding to the residual deformation of 0.2% was considered the yield strength of 18Ni (250). The area reduction Z_i was calculated using Eq. (1):

$$Z_i = \frac{S_i^{'} - S_i}{S_i^{'}}, \; i = 1, 2, 3 \tag{1}$$

where S_i is the cross-sectional area of the sample fracture section, and $S_i^{'}$ is the original section area of the testing section. Mechanical properties of 18Ni (250) that were measured in the

TABLE 1

Chemical composition of the 18Ni (250) maraging steel

Material	Nominal composition (wt.-%)									
	C	Si	Mn	S	P	Ni	Co	Mo	Al	Ti
18Ni (250)	0.008	0.02	0.03	0.001	0.005	17.86	7.93	5.20	0.14	0.48

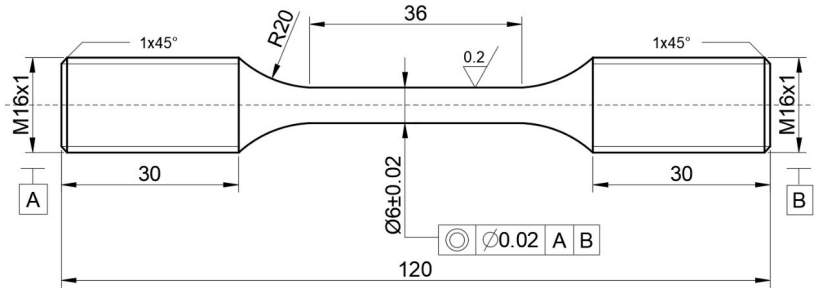

Fig. 1. Geometry of the sample used for evaluating the mechanical properties

tests are listed in Table 2. Where σ_y is the yield strength; E is Young's modulus; σ_b is the ultimate tensile strength; Z/% is the reduction in area; and A/% represents elongation.

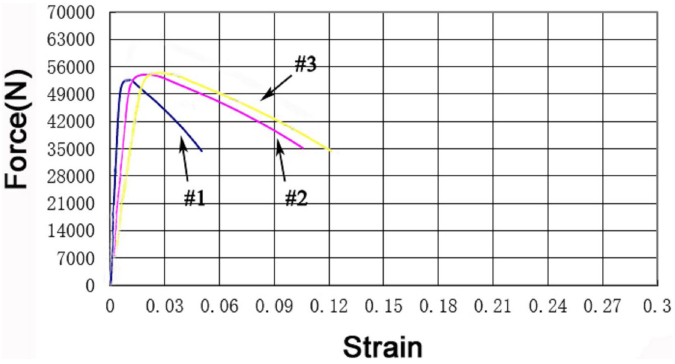

Fig. 2. Force-strain curve of 18Ni (250)

TABLE 2

Mechanical properties of 18Ni (250)

Sample	σ_y/MPa	E/GPa	σ_b/MPa	Z/%	A/%
#1	1800	181	1870	63.1	10
#2	1840	182	1900	66.1	10.5
#3	1860	183	1930	64.2	10.5
Average	1833	182	1900	64.5	10.3

2.2. Axial fatigue test

The sample that exhibited axial fatigue was a round rod, and the shape and sizes are displayed in Fig. 3. The sample gauge was polished with emery paper, and the polishing direction was parallel to the axial direction of the sample. To ensure an accurate result, each group of tests were conducted twice, and the two samples obtained were defined as #1 and #2. In an actual study, most researchers selected 3.5% NaCl solution [18-20] or natural seawater [21] as a corrosion solution, the solution used in this study was 3.5% NaCl solution. The axial fatigue tests were conducted on an electrohydraulic closed-loop servo test machine (MTS880, MTS, USA). The testing machine was equipped with a self-designed NaCl solution circulation system, which comprised a test box, rubber hose, and NaCl solution, as shown in Fig. 4. The test box used for corrosion fatigue was fabricated using PMMA. The NaCl solution entered the test box through the rubber tube by using a pump. When the liquid level in the test box reached the appropriate height, the NaCl solution flowed out through the outlet into the vessel to maintain a stable liquid level.

Axial fatigue tests were conducted at room temperature in air and 3.5% NaCl solution, and the load waveform was sinusoidal. The tests were continued until complete failure of the samples. When the frequency was between 1 and 100 Hz, the frequency had no obvious effect on the fatigue behavior of steels at room temperature in air. Considering experimental efficiency, the loading condition in air was set: f = 10 Hz and R = 0.5. There were three loading conditions for the 3.5% NaCl solution: f = 1 Hz and R = 0.5; f = 1 Hz and R = 0.1; and f = 5 Hz and R = 0.5. The applied stresses were $0.5\sigma_y$, $0.6\sigma_y$, $0.75\sigma_y$, $0.9\sigma_y$, $1.01\sigma_y$, respectively. That's 918 MPa, 1102 MPa, 1378 MPa, 1653 MPa, 1855 MPa. A total of 20 groups were set up in the test scheme, as shown in Table 3. The input data was sinusoidal load with different σ_{max}, R, and f, and output data was fatigue cycle. After the tests, the working sections of the samples were cut off, the fractures were observed along with spectrum analysis using a tungsten filament scanning electron microscope (JSM-6480). The crack initiation site of the side of the sample was observed using a laser microscope (VK-X1000).

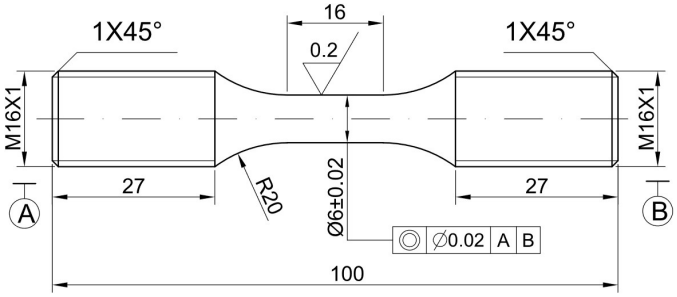

Fig. 3. Sample of axial stress fatigue

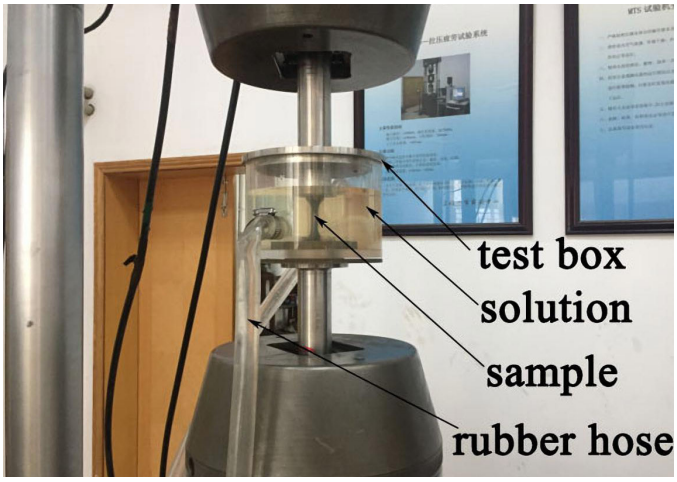

Fig. 4. MTS880 material test system

3. Effect of the Loading Frequency f and the Stress Ratio R

The loading cycles required for failure of 18Ni (250) under different loading conditions are listed in Table 3. The fitted S-N curves of 18Ni (250) with loading frequencies f of 10 Hz in air and 1 Hz in 3.5% NaCl solution are presented in Fig. 5. The y coordinate corresponded to the stress amplitude σ_{MAX}. As presented in Fig. 5, the lower the stress is, the higher the fatigue cycle is. However, with a decrease in stress, the slope of the S-N curve in air tended to decrease gradually. When the stress amplitude was near to half of the yield strength, the fatigue cycle exceeded 10^5 cycles, which fallen within the high-cycle fatigue region.

TABLE 3

Fatigue cycles in air and in the 3.5% NaCl solution

Scheme	σ_{max} / MPa	R	f / Hz	Test environment	Fatigue cycle		
					#1	#2	Average
1	918	0.5	10	Air room temperature	199867	152252	176060
2	1102				75897	74014	74956
3	1378				25396	38111	31754
4	1653				19195	17989	18592
5	1855				6555	13424	9990
6	918	0.5	1	3.5% NaCl solution room temperature	25664	34782	30223
7	1102				22701	27932	25317
8	1378				20067	17033	18550
9	1653				9885	10440	10163
10	1855				7820	6944	7382
11	918	0.1	1		12239	15063	13651
12	1102				10405	9363	9884
13	1378				5874	5853	5864
14	1653				3500	3967	3734
15	1855				1971	2827	2399
16	918	0.5	5		62340	67006	64673
17	1102				48363	—	48363
18	1378				21600	22087	21844
19	1653				12948	12514	12731
20	1855				8570	8013	8292

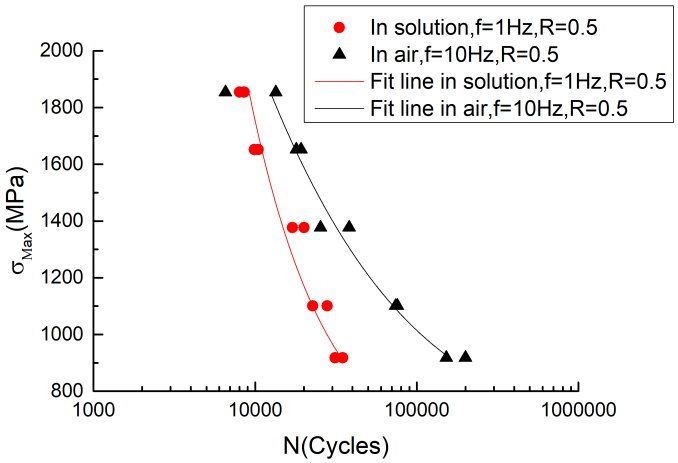

Fig. 5. S-N curves (survival probability Ps = 0.5) of 18Ni (250) in air and 3.5% NaCl solution

As seen in Table 3 and Fig. 5, the curvature of the S-N curve did not exhibit an obvious decreasing tendency in the 3.5% NaCl solution with a decrease in stress. Moreover, the number of fatigue cycles were lower than 10^5 cycles at any stress amplitude. At the same stress amplitudes, the fatigue cycles in the 3.5% NaCl solution were approximately one order of magnitude lower than those in air. For example, when the stress amplitude was 918 MPa, the average fatigue life in air was 1.76×10^5 cycles. Moreover, the average fatigue life in the 3.5% NaCl solution was 3.02×10^4 cycles, which is an 82.8% decrease. The fatigue life in the 3.5% NaCl solution was greatly reduced by the corrosion solution, which directly reflected the poor corrosion resistance of 18Ni (250) in the 3.5% NaCl solution.

The process of corrosion fatigue fracture can be divided into two stages: crack initiation and crack propagation. When the crack length a_0 = 0.25 mm, it is considered that the crack has initiated. Under the continuous action of axial load, cracks initiated and the tips of the cracks were in direct contact with the solution. Due to further stretching, cracks gradually propagated until the sample fractured. The solution shortened the initiation time of cracks. Due to the opening at the crack tip, the solution continuously corroded the fresh metal at the crack tip. This accelerated the crack propagation rate.

The corrosion fatigue life of the sample was affected by two factors – mechanical damage due to the load and corrosion damage due to the 3.5% NaCl solution. The corrosion damage at a specific applied stress amplitude σ_{MAX} (918, 1101, 1377, 1652, and 1854 MPa) was defined as N_D, which was calculated using Eq. (2):

$$N_D = \frac{N_{Air} - N_{NaCl}}{N_{Air}} \tag{2}$$

where N_{Air} is the average fatigue cycle of samples in air at a specific applied stress amplitude (f = 10 Hz, R = 0.5), and N_{NaCl} is the average fatigue cycle of samples in the 3.5% NaCl solution at a specific applied stress amplitude (f = 1 Hz, R = 0.5). The corrosion damage N_D is presented in Table 4 and Fig. 6. With an increase in σ_{MAX}, the corrosion damage N_D gradually decreased. This behavior indicates that the effect of the 3.5% NaCl solution on the fatigue behavior of 18Ni (250) was more significant at small stress amplitudes because the corrosion reaction between the solution and material lasted longer at small stress amplitudes. Moreover, Fig. 5 presents that the smaller the stress amplitude

is, the larger the difference in the fatigue cycles is between the 3.5% NaCl solution and air. A small stress amplitude contributed to a large fatigue cycle, which also meant that the crack tip of sample had a long contact time with the solution, so the corrosion was more sufficient and the corrosion damage was more serious, which was the reason why N_D is large at a small stress amplitude. The more sufficient the corrosion is, the faster the crack propagation is and the more obvious the fatigue cycle reduction is.

TABLE 4

Effect of corrosion on fatigue cycles

σ_{max}/MPa	918	1101	1377	1652	1854
N_D	0.83	0.66	0.42	0.45	0.26

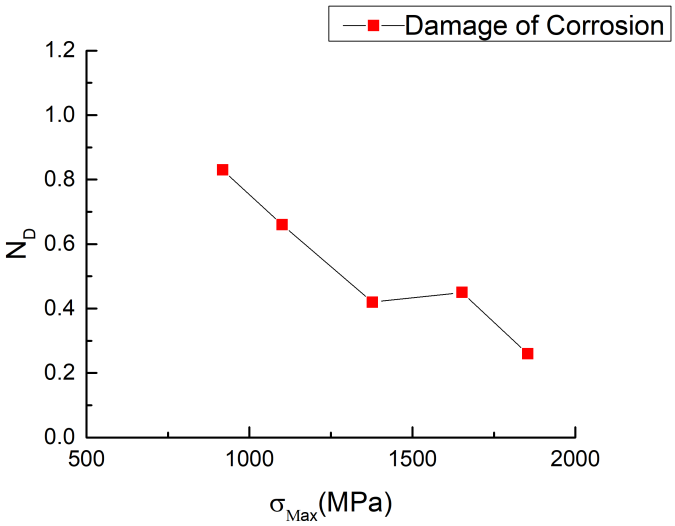

Fig. 6. Corrosion damage

The fitted S-N curves of 18Ni (250) under three loading conditions: f = 5 Hz and R = 0.5, f = 1 Hz and R = 0.1, and f = 1 Hz and R = 0.5 in the 3.5% NaCl solution are shown in Fig. 7. Here, the S-N curve under the conditions of f = 5 Hz and R = 0.5 was considered as the reference. Moreover, the control

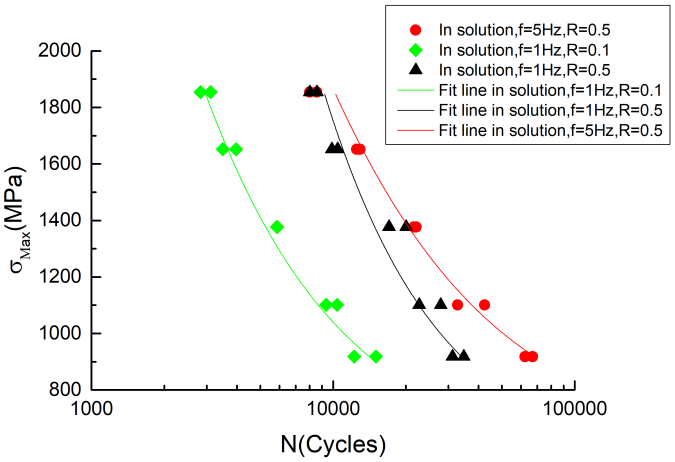

Fig. 7. S-N curves (survival probability Ps = 0.5) of 18Ni (250) in the 3.5% NaCl solution

variable method was employed to study the effect of loading frequency and stress ratio on the corrosion fatigue of 18Ni (250).

At a stress ratio R of 0.5 and when the loading frequency f increased from 1 to 5 Hz, the corrosion fatigue life of 18Ni (250) was significantly improved. For example, when the stress amplitude was 918 MPa, the average fatigue cycles were 3.02×10^4 at f = 1 Hz and the average fatigue cycles were 6.51×10^4 at f = 5 Hz, which is a 115.4% increase. When the loading frequency increased, the mechanical damage due to the load was evident. However, the corrosion damage due to the 3.5% NaCl solution was relatively decreased (the primary reason was that the high frequency made the contact between the solution and crack tip insufficient). Thus, the crack propagation rate decreased and the corrosion fatigue life increased.

At the loading frequency f of 1 Hz and when the stress ratio R decreased from 0.5 to 0.1, the corrosion fatigue life of 18Ni (250) reduced significantly. For example, when the stress amplitude was 918 MPa, the average fatigue cycles at an R value of 0.5 was 3.02×10^4. Moreover, the average fatigue cycles at an R value of 0.1 were 1.37×10^4, which is a 54.8% reduction. The difference between the fatigue strengths obtained at the two stress ratios was large for the short-life condition but small for the long-life condition. The reason for this behavior was that the applied stress was relatively larger for a short-life than that for a long-life. Moreover, the mechanical damage on the material was much larger than corrosion damage caused by the 3.5% NaCl solution.

At a specific applied stress amplitude σ_{MAX} (918, 1101, 1377, 1652, and 1854 MPa), the ratio of life improvement caused by frequency increase was defined as N_f, the ratio of life reduction caused by stress ratio decrease was defined as N_R. Both values were calculated using Eq. (3) and Eq. (4):

$$N_f = \frac{N_{\mathrm{NaCl1}} - N_{\mathrm{NaCl}}}{N_{\mathrm{NaCl}}} \tag{3}$$

$$N_R = \frac{N_{\mathrm{NaCl}} - N_{\mathrm{NaCl2}}}{N_{\mathrm{NaCl}}} \tag{4}$$

where N_{NaCl}, N_{NaCl1}, and N_{NaCl2} were the average fatigue cycles under the specific loading conditions of f = 1 Hz and R = 0.5, f = 5 Hz and R = 0.5, and f = 1 Hz and R = 0.1. The conditions of N_f and N_R are presented in Table 5 and Fig. 8, respectively. The value of N_f exhibited a significant reduction trend and a large span with increase in σ_{MAX}, which indicated that the fatigue life improvement caused by frequency increase was unstable. The value of N_R was relatively stable, constant at approximately 0.6, with an increase in σ_{MAX}. This indicated that the reduction in fatigue life due to stress ratio reduction was stable and did not fluctuate greatly with change in σ_{MAX}. Compared with effect of frequency f, the effect of stress ratio R on 18Ni (250) fatigue life was relatively controllable, which was a great feature of 18Ni (250). In actual applications of offshore structures, either frequency f and stress ratio R could be improved for increasing the corrosion fatigue life of offshore structures made of 18Ni (250). However, increasing the stress ratio R was the better choice.

TABLE 5

Effect of loading frequency and stress ratio on fatigue cycles

σ_{MAX}/MPa	918	1101	1377	1652	1854
N_f	1.15	0.91	0.18	0.25	0.12
N_R	0.55	0.61	0.68	0.63	0.68

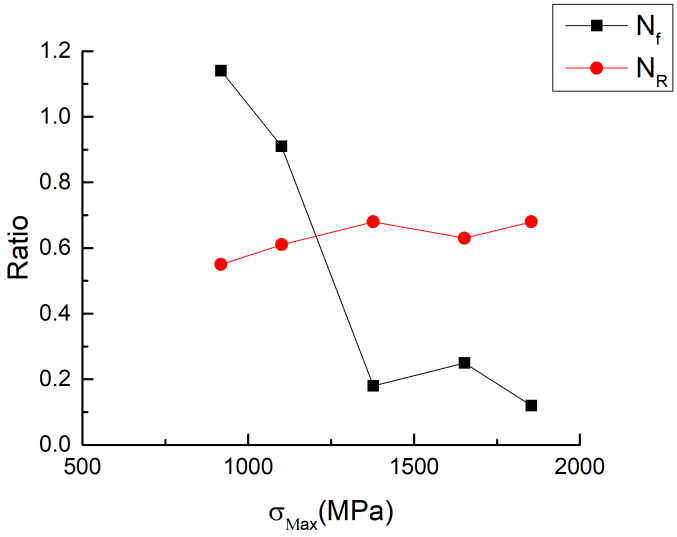

Fig. 8. Effect of loading frequency f and stress ratio R

4. Microstructure Observations

4.1. Fractographic observations

As can be seen in Fig. 9a (918MPa, 3.5%NaCl solution) displays obvious corrosion pits, Fig. 9b (1855MPa, 3.5%NaCl solution) displays serious mechanical tearing. At large stress, the mechanical damage on the material was much larger than corrosion damage. Fig. 10 and Fig. 11 display the crack initiation site of the 18Ni (250) samples at a stress amplitude σ_{MAX} of 1102 MPa, under different test environments (air or 3.5% NaCl solution), and under different loading conditions (f = 5 Hz and R = 0.5, f = 1 Hz and R = 0.5, and f = 1 Hz and R = 0.1). Fig. 10 shows that dimples were distributed on the fatigue fracture of the sample tested in air (Fig. 10a), the fatigue striation propagated like a wave which initiated at the defects. The detailed fractographic features of the sample tested in air can be seen in Fig. 11a, short curved tearing ridges were distributed surrounding the dimples, which indicated that the fatigue crack propagated in the mode of quasi-cleavage on the crack initiation site.

However, for the samples treated in the 3.5% NaCl solution, dimples disappeared, and fractographic features of the samples tested under different loading conditions were very different. Fig. 10b (f = 5 Hz and R = 0.5) displays extensive slips, and detailed fractographic features in Fig. 11b (f = 5 Hz and R = 0.5) displays obvious crack merging. Observing the Fig. 11c, extensive slips were replaced by small slips, and scattered intergranular cracks were found surrounding the slips. This indicated anodic dissolution of dislocation caused by 3.5% NaCl solution, then intergranular cracks formed with the effect of cyclic loadings. In what period, the brittleness of 18Ni(250) increased, and the lower the frequency, the higher the brittleness, the primary reason was that the lower frequency made the dissolution more sufficient. Observing the Fig. 10d (f = 1 Hz and R = 0.1) and Fig. 11.d (f = 1 Hz and R = 0.1), the crack initiation site was relatively flat, slips and dislocations disappeared, where were distributed dense intergranular cracks. Combined with the above, the corrosion fatigue life of the sample was the shortest under the loading conditions of f = 1 Hz and R = 0.1, indicating that the corrosion fatigue life of the sample was greatly shortened by the intergranular cracking, and the intergranular cracking was more likely to occur with a small frequency and a small stress ratio. Analyzing Fig. 10 and Fig. 11, brittleness of 18Ni (250) gradually increased from a to b to c to d.

Fig. 12 presents the crack initiation site of the side of the 18Ni (250) sample at a stress amplitude σ_{MAX} of 1102 MPa, under different test environments (air and 3.5% NaCl solution), and under different loading conditions (f = 1 Hz and R = 0.5, f = 5 Hz and R = 0.5, and f = 1 Hz and R = 0.1). Fig. 12 shows a series of parallel striations that are distributed on the side of the sample, which can be attributed to the applied load cycle. In air, the characteristics of ductile tearing and fibrous metal

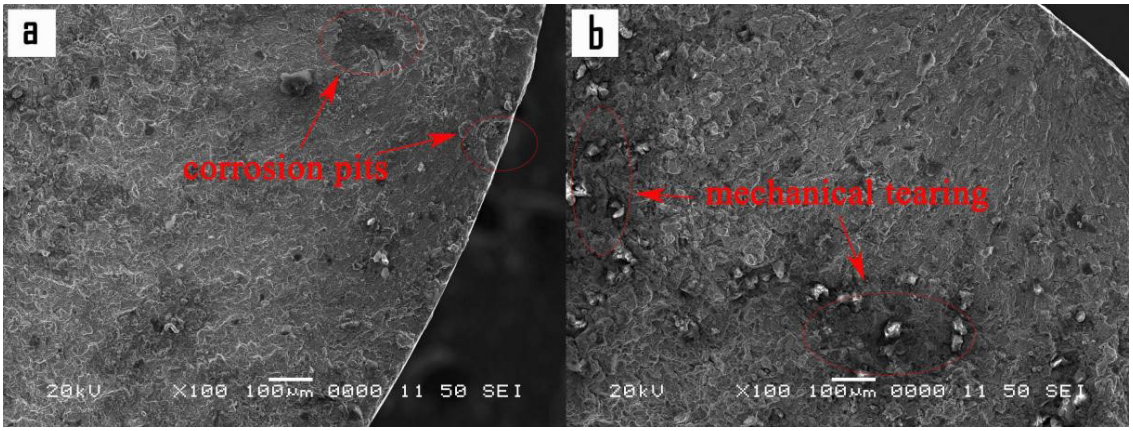

Fig. 9. Fracture features of the samples at f = 1 Hz, R = 0.1 (100 times): (a) 918MPa, 3.5%NaCl solution, (b) 1855MPa, 3.5%NaCl solution

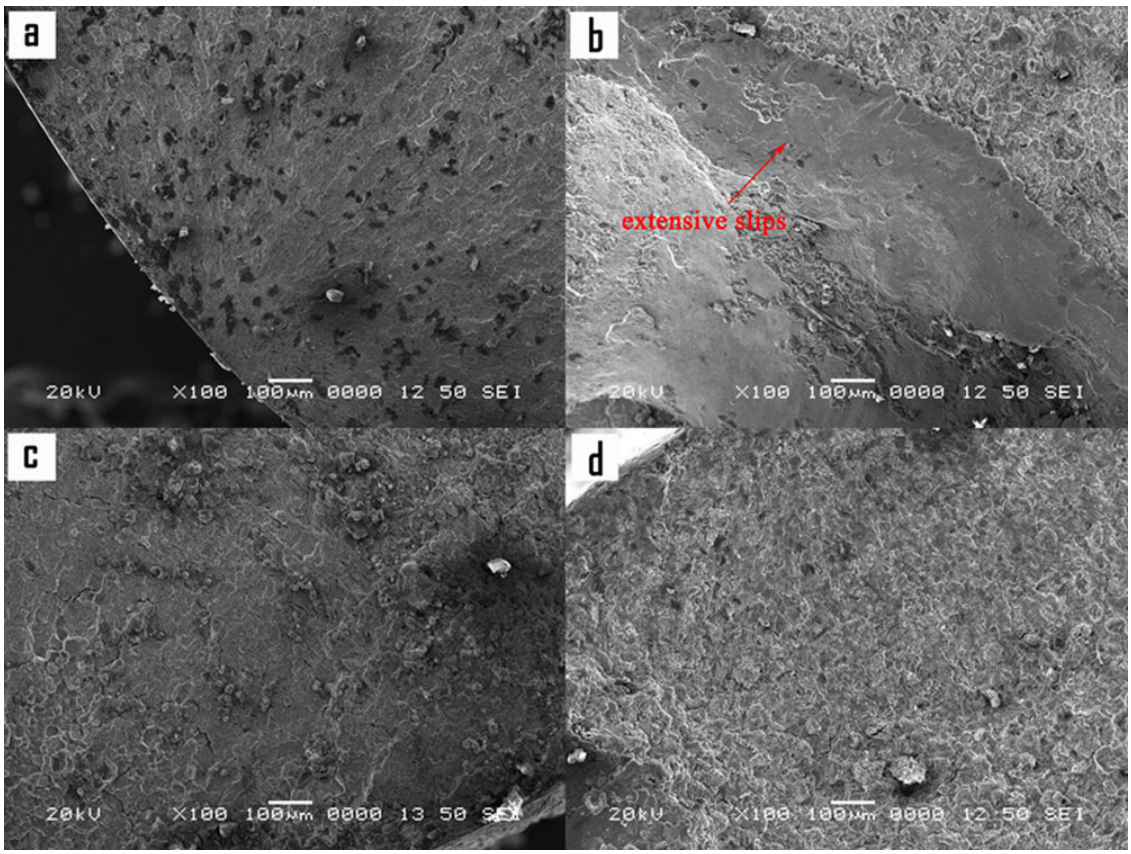

Fig. 10. Fracture features of the samples at 1102 MPa (100 times): (a) f = 10 Hz, R = 0.5 in air, (b) f= 5Hz, R = 0.5 in 3.5%NaCl solution, (c) f = 1 Hz, R = 0.5 in 3.5%NaCl solution, (d) f = 1 Hz, R = 0.1 in 3.5%NaCl solution

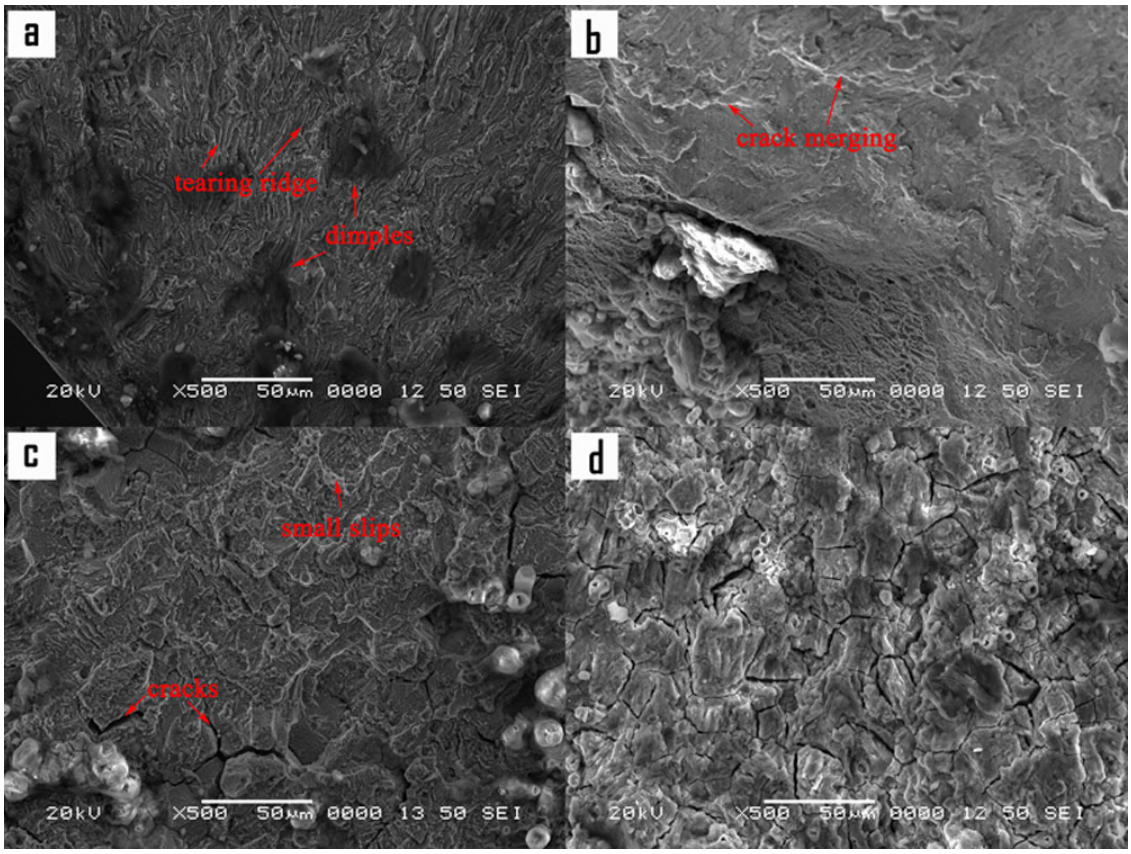

Fig. 11. Fracture features of the samples at 1102 MPa (500 times): (a) f = 10 Hz, R = 0.5 in air, (b) f = 5 Hz, R = 0.5 in 3.5%NaCl solution, (c) f = 1 Hz, R = 0.5 in 3.5%NaCl solution, (d) f = 1 Hz, R = 0.1 in 3.5%NaCl solution

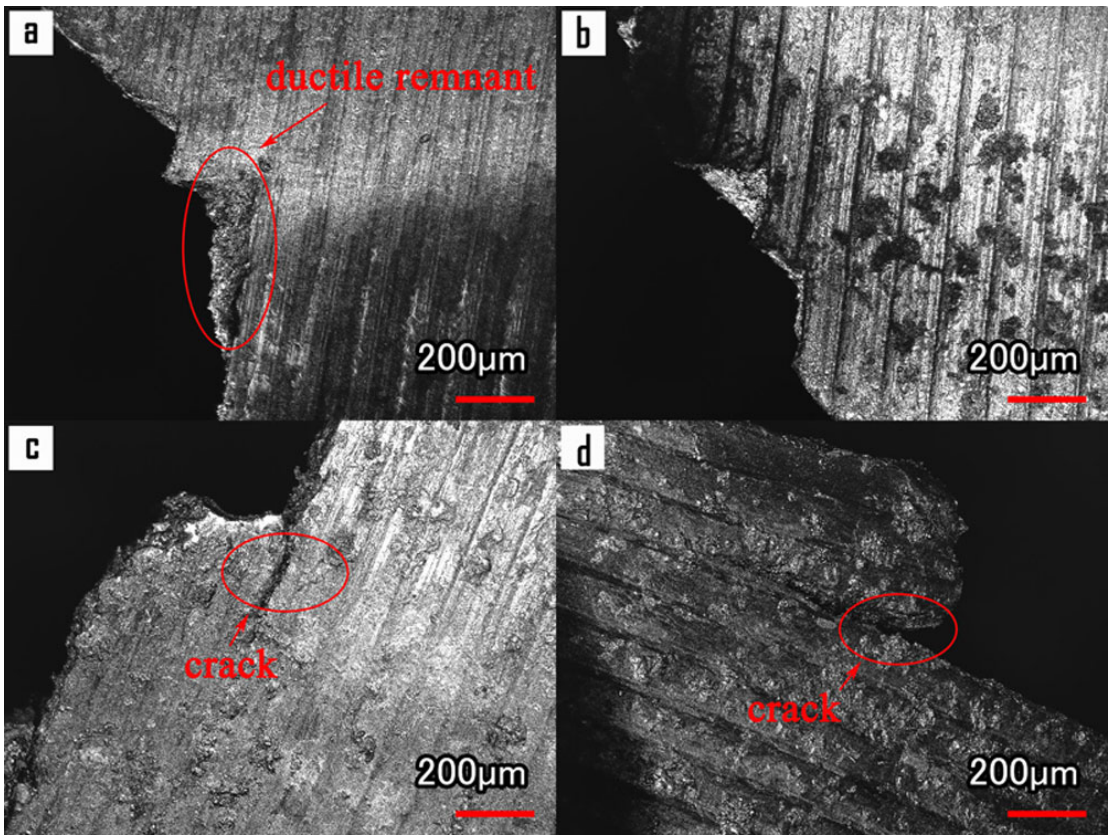

Fig. 12. Side of the fracture at 1102 MPa: (a) f = 10 Hz, R = 0.5 in air, (b) f = 5 Hz, R = 0.5 in 3.5%NaCl solution, (c) f = 1 Hz, R = 0.5 in 3.5%NaCl solution, (d) f = 1 Hz, R = 0.1 in 3.5%NaCl solution

residue were observed on the crack initiation site of the side of the sample (Fig. 12a). In the 3.5% NaCl solution, cracks extended along the striations on the surface of sample, and corrosion pits on the surface of sample were visible. This indicated that the crack initiated from the corrosion pit on the surface and then extended toward the internal region of the sample (indicated by arrows in Fig. 12c-d).

4.2. Spectrum analysis

The spectrum analysis was performed with a tungsten filament scanning electron microscope (JSM-6480). Fig. 13 presents the spectrum analysis of the crack initiation site of the 18Ni (250) sample at a stress amplitude σ_{MAX} of 1102 MPa (in air), and atomic content is presented in Table 6. Fig. 14 presents the spectrum analysis of the crack initiation site tested at a stress amplitude σ_{MAX} of 1102 MPa (in 3.5% NaCl solution, f = 1 Hz and R = 0.5), and atomic content is presented in Table 7. Comparing the two spectrum analysis results, both in air and in solution, the number of atoms ratio of Ni to Fe was about 0.2, showing no significant difference. However, the number of atoms ratio of O to Fe were significantly different, where 0.8 in air and1.3 in solution. O increased obviously under corrosion fatigue, which indicated an oxygen corrosion. The oxygen corrosion promoted the corrosion fatigue cracking. The electrochemical reaction of oxygen corrosion is as follows:

Anodic reaction:

$$Fe \rightarrow Fe^{2+} + 2e^{-}$$

Cathodic reaction:

$$O_2 + H_2O + 4e^{-} \rightarrow 4OH^{-}$$

Total reaction:

$$2Fe + O_2 + 2H_2O \rightarrow 2Fe^{2+} + 4OH^{-}$$

Hydrolysis of Fe^{2+}:

$$Fe^{2+} + 2H_2O \rightarrow Fe(OH)_2 + 2H^{+}$$

$$2Fe(OH)_2 \rightarrow 2FeOOH + 2H^{+} + 2e^{-}$$

$$2Fe(OH)_2 \rightarrow Fe_2O_3 + H_2O + 2H^{+} + 2e^{-}$$

TABLE 6

Spectrum analysis of fracture in air

Chemical element	wt. – %	Number of atoms – %
C	40.09	69.96
O	8.66	11.34
K	0.55	0.29
Fe	35.57	13.35
Co	4.46	1.59
Ni	8.13	2.90
Mo	2.55	0.56

TABLE 7

Spectrum analysis of fracture in 3.5%NaCl solution

Chemical element	wt. – %	Number of atoms – %
C	14.99	35.88
O	16.87	30.31
Ti	0.63	0.38
Fe	46.57	23.98
Co	5.31	2.59
Ni	11.43	5.60
Mo	4.19	1.26

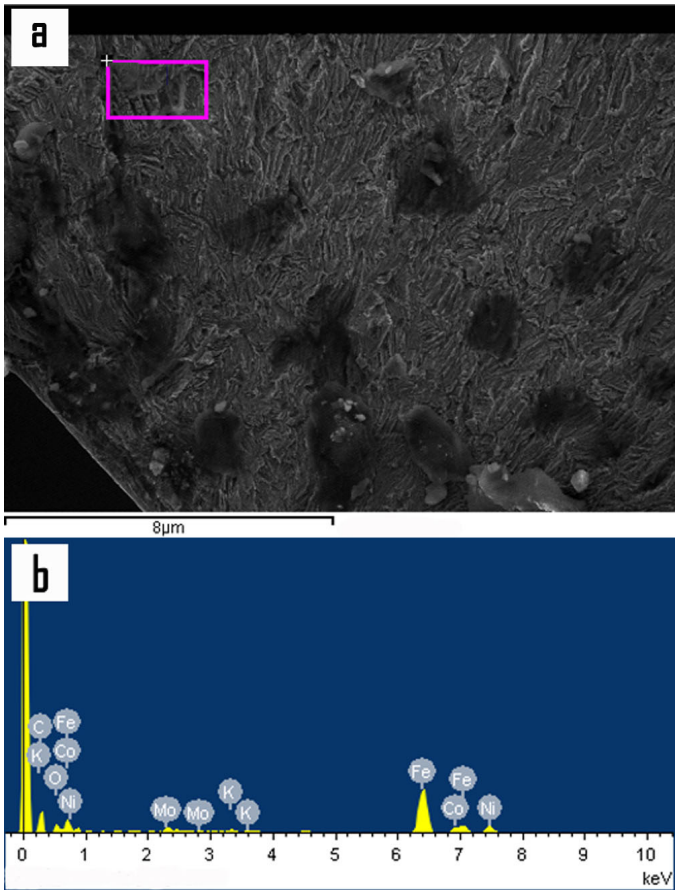

Fig. 13. Spectrum analysis of fracture in air

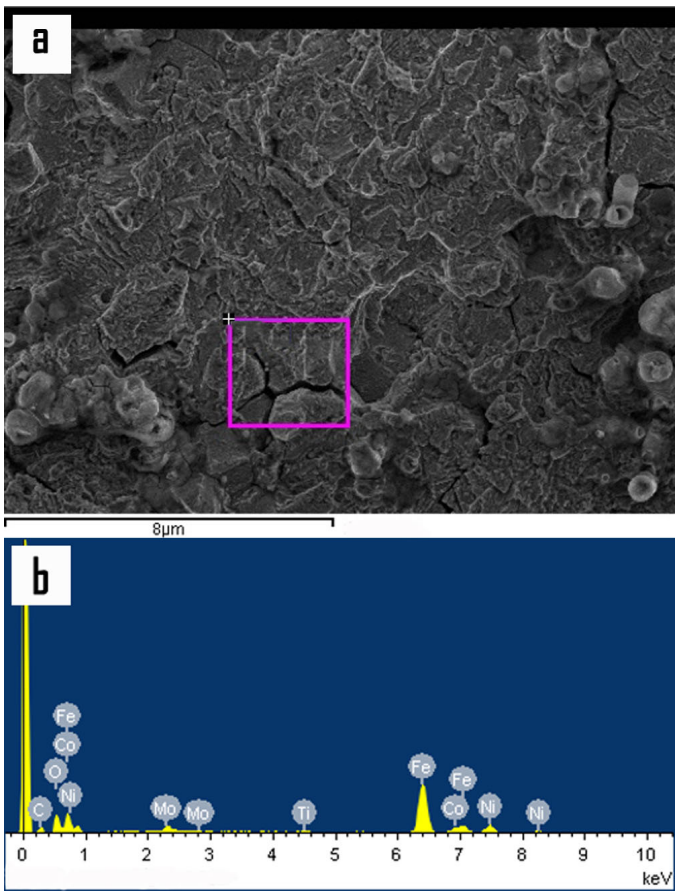

Fig. 14. Spectrum analysis of fracture in 3.5%NaCl solution

5. Conclusions

In this study, the fatigue and corrosion fatigue behavior of 18Ni (250) maraging steel were systematically studied. Moreover, the effect of applied load (loading frequency and stress ratio) on the corrosion fatigue behavior of 18Ni (250) was studied in detail. The main conclusions were summarized as follows:

(1) At the same stress amplitude, the fatigue life of 18Ni (250) in the 3.5% NaCl solution was much shorter than that in air. Moreover, the fatigue life difference between the two samples was approximately one order of magnitude at a small-stress amplitude ($0.5\sigma_y$), which reflected the poor corrosion resistance of 18Ni (250). 18Ni (250), which is an alternative material for fabricating a full ocean depth pressure device, has the advantage of ultrahigh strength and the disadvantage of poor corrosion resistance.

(2) The stress amplitude of 18Ni (250) has a great influence on the corrosion fatigue behavior. As the stress amplitude σ_{MAX} increased, the corrosion damage N_D gradually decreased from 0.83 to 0.26. The corrosion damage at 918 MPa ($0.5\sigma_y$) was 84% greater than that at 1653 MPa ($0.9\sigma_y$). The corrosion of the 3.5% NaCl solution on 18Ni (250) was more significant at a small stress, which was due to the sufficient contact between the solution and crack tip.

(3) With an increase in the loading frequency f, the corrosion fatigue life of 18Ni (250) improved significantly. When the loading frequency increased from 1 to 5, the corrosion fatigue life approximately doubled at 918 MPa ($0.5\sigma_y$). The mechanical damage of load was more evident as the loading frequency was increased, and the corrosion damage was relatively weakened (solution and crack tip contact insufficiently). This finding was different from reference [10]: a loading frequency in the range from 10 to 120 Hz had no appreciable effect on X12CrMoV12-3, which was related with passivation of martensitic stainless steel.

(4) The effect of stress ratio on the corrosion fatigue life was more stable than the effect of loading frequency on the corrosion fatigue life, which was a great feature of 18Ni (250). With an increase in the stress amplitude σ_{MAX}, the value of N_R stabled at approximately 0.6, while N_f exhibited

a significant reduction trend and a large span. Increase in the loading frequency *f* or stress ratio *R* could improve the corrosion fatigue life of 18Ni (250). However, increasing the stress ratio *R* was the better choice.

(5) In air, crack propagated in the mode of quasi-cleavage on the crack initiation site. However, for the sample tested in the 3.5% NaCl solution, intergranular cracks increased. Intergranular cracking was more likely to occur with a small frequency and a small stress ratio, which seriously affected the fatigue life of sample.

(6) In air, crack initiated at the defects on the surface and then extended toward the internal region of the sample. While, in solution, crack initiated at the corrosion pits. O increased obviously under corrosion fatigue, oxygen corrosion occurred in the 3.5% NaCl solution, which promoted the corrosion fatigue cracking.

Acknowledgements

This study was funded by the General Program of National Natural Science Foundation of China ('Study on the Design and Life Calculation Method for the Maraging Steel Sphere of Full-ocean-depth Manned Submersible' (Grant No. 51679133); the State Key Program of National Natural Science of China ('Structural Reliability Analysis on the Spherical Hull of Deepsea Manned Submersibles;' Grant No. 51439004), the Natural Science Foundation of the Jiangsu Higher Education Institutions of China (Grant No.19KJA530002), and Graduate Research and Practice Innovation in Jiangsu Province (Grant No. SJCX19_0608).

REFERENCES

[1] W.M. Zhao, Y.X. Wang, T.M. Zhao, Y. Wang, Corros. Sci. **57**, 99-103 (2012).

[2] J.B. Tan, X.Q. Wu, E.H. Han, W. Ke, X.Q. Liu, F.J. Meng, X.L. Xu, Corros. Sci. **89**, 203-213 (2014).

[3] O. Adedipe, F. Brennan, A. Kolios, Renew. Sust. Ener. **61**, 141-154 (2016).

[4] Z.Y. Zhang, J.B. Tan, X.Q. Wu, E.H. Han, W. Ke, J.C. Rao, Corros. Sci. **146**, 80-89 (2019).

[5] G.P. Guslyakova, S.I. Zhbannikov, G.V. Pachurin, Mater. Sci. **28**, 182-185, (1993).

[6] N. Chapman, L. Brooking, J. Sumner, S. Gray, J. Nicholls, Mater. High Temp. **35**, 151-158 (2017).

[7] T. Michler, J. Naumann, J. Wiebesiek, E. Sattler, Int. J. Fatigue **96**, 67-77 (2017).

[8] J.P. Strizak, H. Tian, P.K. Liaw, L.K. Mansur, J. Nucl. Mater. **343**, 134-144 (2005).

[9] C. Colombo, G. Fumagalli, F. Bolzoni, G. Gobbi, L. Vergani, Int. J. Fatigue **83**, 2-9 (2016).

[10] M.E. May, T. Palin-Luc, N. Saintier, O. Devos, Int. J. Fatigue **47**, 330-339 (2013).

[11] O. Adedipe, F. Brennan, A. Kolios, Mar. Struct. **42**, 115-136 (2015).

[12] R.M. Bay, D.J. Schrock, A.M. Akman, L.G. Bland, R. Thodla, J.S. Locke, Int. J. Fatigue **124**, 1-9 (2019).

[13] A. Trudel, M. Sabourin, M. Lévesque, M. Brochu, Int. J. Fatigue 66, 39-46 (2014).

[14] Z.Q. Hua, S.S. Wu, J. Mater. Res. **30**, 833-840 (2015).

[15] S. Sivaprasad, S. Tarafder, V.R. Ranganath, M. Tarafder, K.K. Ray, Corros. Sci. **48**, 1996-2013 (2006).

[16] F. Wang, Y. Hu, W.C. Cui, J. Ship Mech. **12**, 1557-1572 (2016).

[17] S.J. Zhang, F. Wang, W.C. Cui, J. Ship Mech. **22**, 1540-1548 (2018).

[18] Q. Guo, J.H. Liu, M. Yu, S.M. Li, Appl. Surf. Sci. **327**, 313-320 (2015).

[19] N. Micone, W.D. Waele, Exp. Mech. **57**, 547-557 (2017).

[20] W. Wang, R.Q. Xu, Y.X. Hao, Q. Wang, L.L. Yu, Q.Y. Che, J. Cai, K.S. Wang, Z.Y. Ma, J. Mater. Sci. Technol. **34**, 148-156 (2018).

[21] H. Möller, E.T. Boshoff, H. Froneman, J. S. Afr. I. Min. Metall. **106**, 585-592 (2006).